

Assessment of the relative tectonic activity in the Bailongjiang Basin: insights from DEM-derived geomorphic indices

Zhiyang Chang^{1,2} · Weihong Sun³ · Jian Wang²

Received: 18 January 2015 / Accepted: 11 May 2015 / Published online: 24 May 2015
© Springer-Verlag Berlin Heidelberg 2015

Abstract The Bailongjiang drainage basin is located in the transition zone between the Tibetan Plateau and the Loess Plateau. Active tectonic records demonstrate the interplay between the Tibetan Plateau uplift and the different movement of the faults. To assess the relative tectonic activities in this area, five geomorphic indices derived through geographic information system were analyzed: the stream-gradient index (SL), hypsometric integral (HI), valley floor width–valley height ratio (VF), drainage basin shape, and drainage basin asymmetry (AF). Active faults, seismogenic activity, and river terraces were also integrated into this investigation. The results indicate that four classes of relative tectonic activity were defined: Class 1 (very high relative tectonic activity, 5.5 % in the area); Class 2 (high, 54 %); Class 3 (moderate, 24.1 %), and Class 4 (low, 16.4 %). Sub-basins at the midstream and upstream of Bailongjiang show abnormally high SL, high HI, AF, and convex hypsometric curves and low VF values due to the impact of the east-ward extrusion of the Tibetan plateau and active faults. The downstream shows low SL, HI, and AF and concave hypsometric curves due to the low tectonic activity of the faults inhibited by Minshan. These results are consistent with the geological background.

Keywords Geomorphic indices · GIS · Tectonic activity level · Bailongjiang drainage basin

Introduction

The geomorphic indexes of active tectonics are known to be useful in active tectonic studies (Bull and McFadden 1977; Azor et al. 2002; Keller and Pinter 1996, 2002; Silva et al. 2003; Giaconia et al. 2012a, b), and the increasing availability of digital elevation models (DEM) and geographic information system (GIS) software has facilitated the large-scale characterization of landscapes (Keller and Pinter 2002; Walcott and Summerfield 2008; Cheng et al. 2012; Bagha et al. 2014). In recent studies related to morpha-tectonics, a mixture of geomorphological and morphometric analyses of land-forms and topographic analyses were utilized to analyze active tectonics. For example, Bull and McFadden (1977) and Silva et al. (2003) studied the relative active tectonics of various mountain fronts based on mountain-front sinuosity (Smf) and the ratio of the valley floor width to the valley height (VF) indexes, and they applied the asymmetric factor (AF) and drainage basin shape (BS) indexes to support tectonic tilting. El Hamdouni et al. (2008) presented a new method to evaluate the relative active tectonics based on geomorphic indices useful in evaluating morphology and topography. Alipoor et al. (2011) used the analytic hierarchy process to develop an integrated quantitative geomorphic analysis of the tectonic activity around the Rudbar Lorestan dam site. Font et al. (2010) and Gao et al. (2013) studied the relationship among the stream length-gradient index (SL), hypsometric integral (HI), the lithology and tectonic uplift in the Normandy intraplate area of NW France and the northeastern margin of the Tibetan Plateau,

✉ Jian Wang
wangjian@njnu.edu.cn

Zhiyang Chang
changzhiyang1@126.com

¹ Nanjing Institute of Tourism & Hospitality,
Nanjing 211100, Jiangsu, China

² College of Geographical Sciences, Nanjing Normal
University, Nanjing 210023, China

³ Jiang Su Province Surveying & Mapping Engineering
Institute, Nanjing 210013, Jiangsu, China

respectively. Giacomia et al. (2012b) used typical geomorphic indices to evidence the active tectonics in the Sierra Alhamilla. There have been other similar attempts to systematically investigate geomorphic response to tectonism with the help of geomorphic indices in various tectonically active areas affected by faults and folds, such as Central Italy (Troiani and Della Seta 2008), the Pacific coast of Costa Rica (Wells et al. 1988), Central Zagros of Iran (Dehbozorgi et al. 2010), the western foothills of the Taiwan Mountains (Chen et al. 2003), and the central and eastern part of the Betic Cordillera (Pedrera et al. 2009; Pérez-Peña et al. 2010). All these studies indicate the applicability of morphometric indices to tectonically active regions.

The Bailongjiang drainage basin is located in the transition zone that is the famous north–south seismic belt of China (Zhang et al. 2010). Several sectors could be differentiated considering the relative tectonic activity level. The aim of this study is to produce a single geomorphic index capable of characterizing the relative tectonic activity within the large sectors and provide an example of its potential in the Bailongjiang drainage basin.

Study area

The Bailongjiang drainage basin covers an area of 31,808 km² and is located in the transition zone between the Tibetan Plateau and the West Qinling Orogen and it is one of the most serious debris flow and landslide disaster areas in China (Bai et al. 2014). The Bailongjiang River is a tributary of the Yangtze River. It has many tributaries of which the largest are the Min River, Beiyu River, and Baishui River. The length of the main stream is approximately 576 km with the relief more than 2783 m, and the mean stream gradient is 4.8 %. The valleys exhibit V-shaped or canyon forms.

This area is influenced by warm and humid subtropical monsoon climate but also experiences orographical effects due to the terrain. The tectonic activity is related to continuous uplift and extension of the Tibetan Plateau since the late Cenozoic (Zhang et al. 2003, 2011). An $M = 8.0$ earthquake in 1879 generated by the Wenxian fault (Zhan 2006) occurred in this region. Additionally, many $M > 7.0$ and $M > 6.0$ earthquakes occurred in the study area between 1831 BC and 2008 AD (Fig. 2). Global positioning system (GPS) measurements indicate that the largest horizontal displacement velocity of this region could reach 42–35 mm/a (Meng et al. 2013).

The regional tectonic system is composed of multiple active faults. In the upper of Bailongjiang, the East Kunlun fault (F1) is given priority with left strike-slip extrusion activity at a rate of approximately 10 mm/a

(Woerd et al. 2002). To the east, the left strike-slip rate of the Tazang fault is 1–1.5 mm/a (Ren et al. 2013). The left strike-slip rate of the West Qinling fault is 2–3 mm/a (Li 2005) from the late quaternary. In the north of the Diebu-Bailongjiang fault, the thrust rate is 0.7 mm/a, whereas the south of this fault has a thrust rate 0.38 ± 0.12 mm/a and a strike-slip 1.37 ± 0.10 mm/a (Liu 2012). The left strike-slip rate of the Guangaishan-Dieshan fault is approximately 0.51 ± 0.13 mm/a with a vertical slip rate of 0.49 ± 0.08 to 1.15 ± 0.28 mm/a (Liu 2012). The strike-slip of the Lintan-dangchang is about 2–2.5 mm/a (Yuan et al. 2004). The left strike-slip fault of Wenxian is about 2–2.5 mm/a from the Holocene (Liu 2012). In the downstream, there has been no activity for the Jiangyou fault and Pingwu-qingchuan fault since quaternary. The seismic activity is low along the Beichuan-linansi fault and there is no obvious activity about this fault since the time of the late Pleistocene (Chen et al. 2007, 2008).

There are four terrace levels in Minxian, five terrace levels in Dangchang, seven terrace levels in Wudu (Guo et al. 2006a, b), and six terrace levels in Zhouqu (Chen and Li 1997) (Fig. 1). These terraces cover a time span of

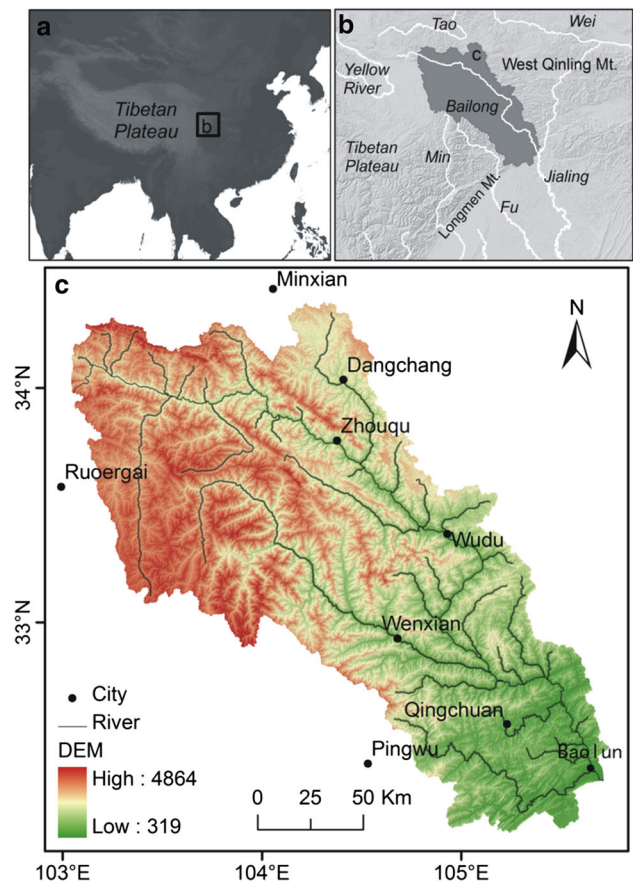


Fig. 1 Location and elevation distribution map of Bailongjiang drainage basin

Table 1 Distribution of rock groups in the study area

Code	Rock group	Characteristics
B	Metamorphic sandstone, metamorphic conglomerate, slate	Metamorphic sandstone, sandy clay slate, sandstone, conglomerate, metamorphic fine sandstone, quartz sandstone
C	Metamorphic andesite, tuff metamorphic, metamorphic basalt	Metamorphic andesite, andesitic basalt, andesitic tuff, basalt porphyry plus chert, tuffaceous sandstone, phyllite
D	Phyllite, slate, thin limestone	Phyllite mix quartzite, sericite phyllite mix tuff, carbonaceous phyllite mix slate, limestone, chert and fine and siltstone
E	Thick layer of limestone, slate	Thick layer of limestone rock in the splint, phyllite, chert, silty and fine, and thick layer of slate, limestone, phyllite, chert and fine and siltstone
F	Thick layer of sandstone, limestone slate	Thick layer of sandstone, slate phyllite, thin argillaceous limestone
G	Thick layer of conglomerate, sandy conglomerate	Thick, thick layer of conglomerate, sandy conglomerate mudstones
H	Siltstone, mudstone, thin sandy conglomerate	Muddy siltstone, silty mudstone in thin muddy sandstone, conglomerate, muddy sandstone
I	Rock sand and gravel	Ancient river bed, modern bed alluvial, alluvial deposits of sand and gravel layers
J	Clay	Loess, loess-like soil
K	Magmatic rocks	Granite, diorite, peridotite

approximately 1.8–0.01 Ma (Li et al. 2001), indicating recent uplift in the area. The uplift rate is approximately 1 mm/a between 0.01 Ma and 0.05 Ma from the perched river terraces (Guo et al. 2006a).

In the study area, a variety of lithological strata are present, such as the Silurian, Devonian, Carboniferous, Permian and Triassic in the Paleozoic, and the Triassic of the Mesozoic and Quaternary. Based on the geological maps at 1:500000 scale, ten lithological units were defined based on their composition and physical–mechanical characteristics (Zhan 2006) (Table 1). Each lithological unit has similar geological properties and conditions. An overview on the 10 lithological units is presented in Fig. 2.

The location of earthquakes and fault traces are based on Gu et al. (1983), Yu et al. (2012), Chen et al. (2007).

Data and methodology

Morphometric indices are used to analyze the landform and to evaluate the degree of tectonic activity in the area. The indices used for active tectonic studies are the Stream length-gradient index (SL), Hypsometric index (HI), Asymmetric factor (AF), Basin shape index (BS), and Ratio of VF. The Shuttle Radar Topography Mission (SRTM) DEM with 90-m resolution was downloaded from <http://srtm.csi.cgiar.org>. The DEM is seamless because voids have been filled by interpolation techniques, and it is used for regional scale geomorphic analysis (Grohmann et al. 2007). The DEM was analyzed using GIS software, which is a fast and inexpensive way to calculate the

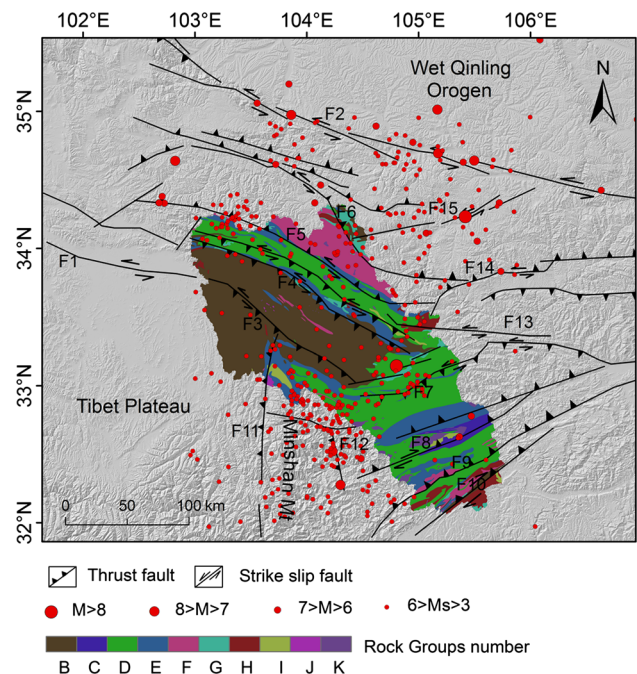


Fig. 2 Distribution of rock group and faults in the study area. Geology was digitized from 1: 500,000 Chinese geologic maps according to Zhan 2006. In the inset, F1 East Kunlun fault, F2 West Qinling fault, F3 Tazang fault, F4 Diebu-Bailongjiang fault, F5 Guanggaishan-Dieshan fault, F6 Lintan-Dangchang fault, F7 Wenxian fault, F8 Qingchuan fault, F9 Beichuan-Linansi fault, F10 Jiangyou fault, F11 Minjiang fault, F12 Huya fault, F13 Kangxian-Lueyang fault, F14 Liangdang-Jiangluo fault, F15 Lixian-Luojiabao fault

morphometric parameters. A total of 33 drainage sub-basins were extracted from the DEM using ArcGIS (v.9.3) software (Fig. 3).

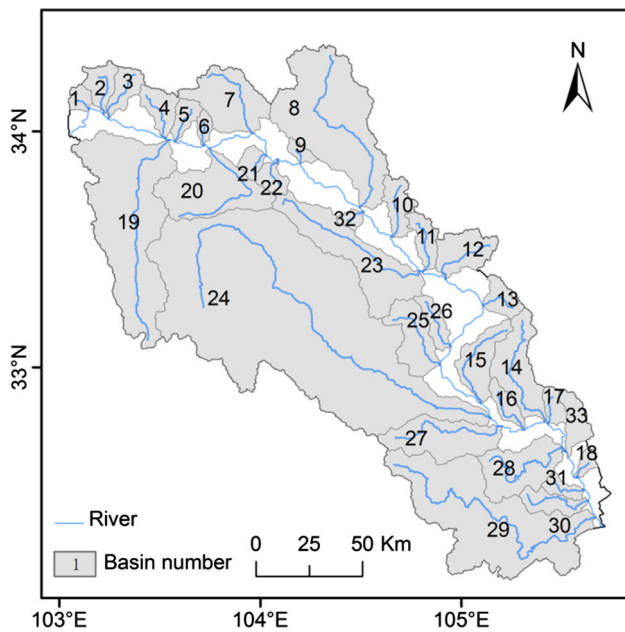


Fig. 3 Map showing 33 sub-basins of Bailongjiang basin

Stream length-gradient index (SL)

The SL index is one of the quantitative geomorphic parameters included in morpho-tectonic assessment (Hack 1973). This index is highly sensitive to changes in the channel slope and rock resistance (Brookfield 1998; Pérez-Peña et al. 2009b), which allows for the association of tectonic activity with rock resistance and topography. The SL is calculated using the following formula (Hack 1973):

$$SL = (\Delta H / \Delta L) \times L, \quad (1)$$

where, SL is stream length-gradient index, ΔH is the change in elevation of reach, ΔL is the length of the reach, and L is the total channel length from the point of interest where the index is being calculated upstream to the highest point on the channel. The SL index can be used to evaluate the relative tectonic activity. High SL index values occur when rivers flow over areas subjected to active uplift or across rocks that are resistant to erosion. In contrast, low SL values are related to stable or subsiding areas. (Keller and Pinter 2002).

Hypsometric integral (HI)

The HI measures the relative distribution of the elevation of a given area of a landscape, particularly a drainage basin (Strahler 1952). This index is defined as the area below the hypsometric curve, and it represents the degree of landscape dissection within a basin. HI values range from 0 to 1. Usually, values close to 0 indicate highly eroded tectonically inactive regions, whereas those close

to 1 indicate slightly eroded tectonically active regions (Keller and Pinter 2002). The shape of the hypsometric curves is related to the degrees of dissection of the basin. Convex hypsometric curves characterize relatively “young” weakly eroded regions, S-shaped curves characterize moderately eroded regions, and concave curves characterize relatively “old” highly eroded regions. The HI values and hypsometric curves provide the information about the tectonic, climatic, and lithological factors controlling the stage of the basin (EI Hamdouni et al. 2008; Pérez-Peña et al. 2010). The HI values and hypsometric curves were calculated for the 33 sub-basins of the Bailongjiang drainage basin with the aid of an ArcGIS extension (CalHypso) developed by Pérez-Peña et al. (2009a).

HI values are dependent on the lithological erosion strength (EI Hamdouni et al. 2008; Gao et al. 2013). These values could be obtained by regular squares of an analysis grid. Because of the large area (31,808 km²) and the variation in the lithology, it is difficult for us to perform a detailed analysis of the erodibility. So we focused on the rock groups (Fig. 2 and Table 1) and 1 km² analysis grid using the 90 m SRTM DEM to correlate the HI values with the lithology. The main lithology based on each 1 km² square of the Bailongjiang drainage basin was calculated to compute the percentage of the lithology appearing more frequently. Only the squares that contained at least 80 % of the main rock group were taken into account, as shown in Fig. 4a (Pérez-Peña et al. 2009c). The mean and the standard deviation of the HI values were obtained in each rock group too.

Asymmetric factor (AF)

The AF is a way to indicate the amount of tilting in a drainage basin. The method may be applied over a relatively large area (Hare and Gardner 1985). It can be calculated as

$$AF = 100 \times (Ar/At), \quad (2)$$

where Ar is the area on the right side of the drainage basin facing downstream, and At is the total area of the drainage basin. Values of AF above or below 50 indicate that the basin is asymmetric, whereas values close to 50 indicate that the basin has little tilting. Structural control, such as active tilting and/or the bedding or foliation attitude, plays a main role in the development of the basin asymmetry (Pérez-Peña et al. 2009a). For the purpose of evaluating the relative tectonic activity, AF was expressed as the absolute value minus 50, with an arrow indicating the asymmetry direction. Assuming the tectonic activity leads to left tilt in a drainage basin, the tributaries in the left side of main stream will be shorter than the right.

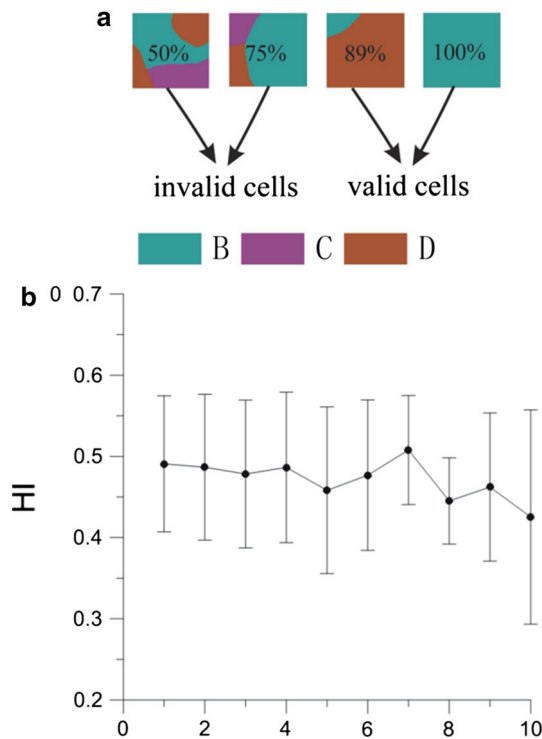


Fig. 4 **a** Schematic showing the selection of valid cells for the lithological analysis. **b** Mean HI values and standard deviations for each lithological group. The numbers 1–10 correspond to B–K in Fig. 2 and Table 1

$$AF = |(Ar/At) \times 100 - 50|. \tag{3}$$

Basin shape index (BS)

The horizontal projection of a basin may be described by the basin shape index or the elongation ratio, BS (Ramirez-Herrera 1998):

$$BS = Bl/Bw, \tag{4}$$

where *Bl* is the length of the basin measured from the headwaters to the mouth, and *Bw* is the width of the basin measured at its widest point. High values of BS are associated with young elongated basins; these basins generally have higher tectonic activity. With the decrease of the tectonic activity and the evolution, the shape of the basins change to circular with lower BS (Bull and McFadden 1977).

Ratio of valley floor width to valley height (VF)

The VF (Bull and McFadden 1977) is a geomorphic index used to differentiate broad-floored, U-shaped valleys from

narrow-floored V-shaped valleys. This index is defined as (Giaconia et al. 2012a, b)

$$VF = 2Vfw/(Eld + Erd - 2Esc), \tag{5}$$

where *Vfw* is the width of the valley floor, *Eld* and *Erd* are the elevations of the left and right valley divides, respectively, and *Esc* is the elevation of the valley floor. Deep V-shaped valleys ($VF < 1$) are connected with linear, active down cutting streams characteristic of areas subjected to active uplift, whereas flat-floored (U-shaped) valleys ($VF > 1$) indicate an attainment of the base level of erosion mainly in response to the relative tectonic quiescence (Keller and Pinter 2002). The method of Mahmood and Gloaguen (2012) was borrowed to take more than one cross sections upstream for VF estimation in case of large basins and then took the average of these values as a representative of that particular basin.

Index of relative active tectonics (Iat)

The average of six geomorphic indices (*Iat*) was used to evaluate tectonics in the southwest border of the Sierra Nevada (EI Hamdouni et al. 2008). Here, *Iat* was just slightly modified using five geomorphic indices except for the index of *Smf* for the impact of the DEM resolution. The values for each geomorphic index were classified into three classes (EI Hamdouni et al. 2008). Next, the results were accumulated and averaged as *Iat*, which we divided into four classes from low to very high tectonic activity with the method of natural breaks.

Results

The necessary parameters were measured from the SRTM using the GIS. The SL values were calculated along the streams on the DEM in GIS, and the average value was calculated for each sub-basin. The range of the average values was from 206 (Sub-basin 31) to 3236 (Sub-basin 24), and the values were graded into three classes: class 1 ($SL \geq 500$); class 2 ($300 \leq SL < 500$); and class 3 ($SL < 300$) according to EI Hamdouni et al. (2008). The distribution of these classes is shown in Fig. 5. Figure 6 shows some of the longitudinal river profiles of the selected sub-basins and their computed SL Values.

The HI values range from 0.24 (sub-basin 31) to 0.62 (sub-basin 11), and can be grouped into three classes with respect to the shape of the hypsometric curves: Class 1 with convex hypsometric curves ($HI \geq 0.5$); Class 2 with concave-convex hypsometric curves ($0.4 \leq HI < 0.5$); and Class 3 with concave hypsometric curves ($HI < 0.4$) (EI

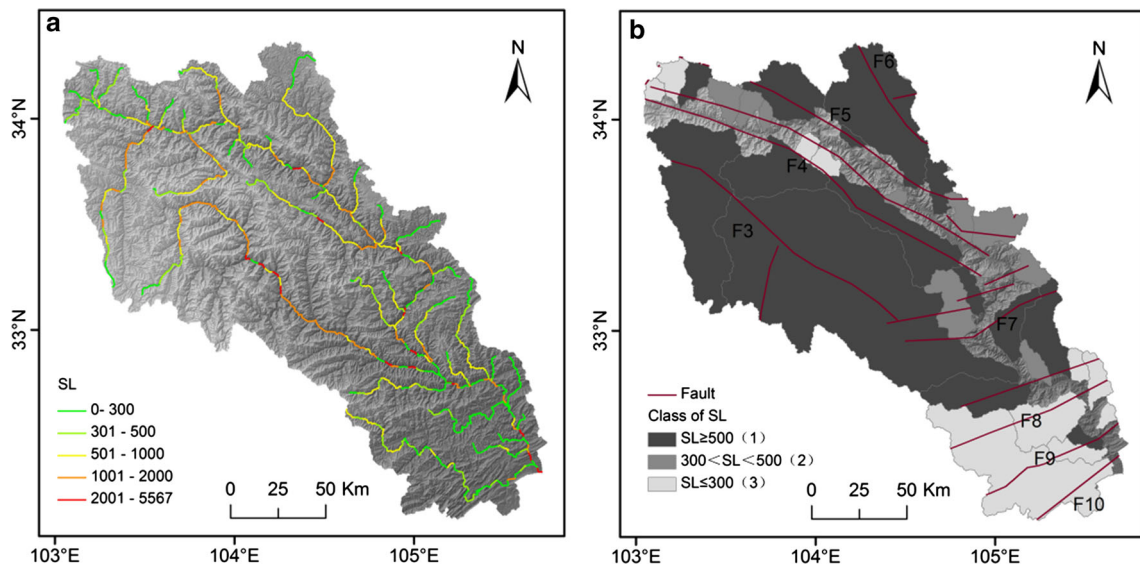


Fig. 5 The distribution of SL and classification

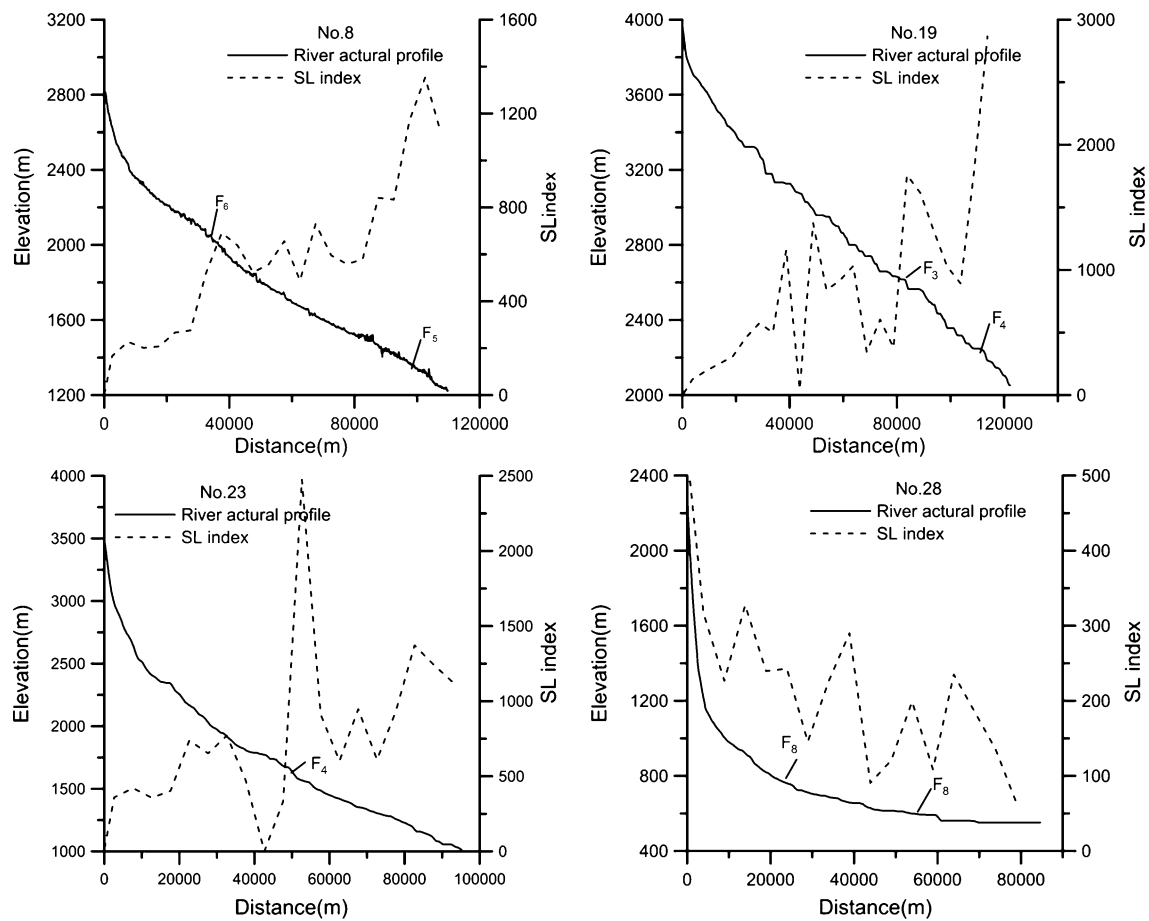


Fig. 6 Some typical river profiles and the indexes of SL

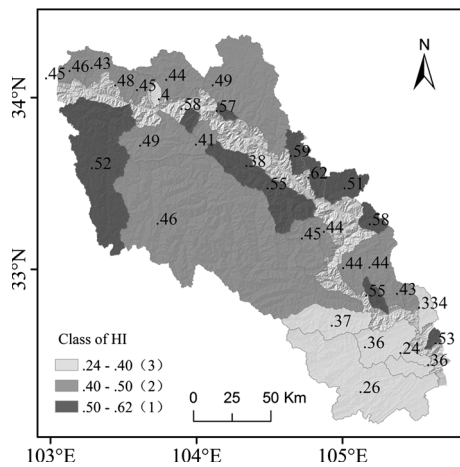


Fig. 7 The values of Hypsometric and classification

Hamdouni et al. 2008) (Figs. 7 and 8; Table 2). Sub-basins found in the upper and middle of the Bailongjiang basin show convex or “S” hypsometric curves with high HI values (sub-basins 10, 11, 12, 13, 19, 23), whereas those found in the downstream of the study area show concave shapes with low HI values (sub-basins 28, 29, 30, and 31).

The values of AF extracted by GIS range from 0.20 (sub-basin 3) to 25.80 (sub-basin 33). We divided the AF absolute values into three classes (Pérez-Peña et al. 2009a): Class 1 with strongly asymmetric basins ($AF \geq 15$), Class 2 with moderately asymmetric basin ($7 \leq AF < 15$), and Class 3 with gently asymmetric basins ($AF < 7$), as shown in Fig. 9 and Table 2. This value in sub-basins 10, 11, 24, 25, 26, 29, and 31 is less than in the other sub-basins. The direction of tilting is shown in Fig. 9.

The BS was calculated using the DEM and was classified into three classes based on the method of natural breaks: class1 ($BS > 2.3$), class 2 ($1.5 \leq BS \leq 2.3$), and class 3 ($BS \leq 1.5$) (Fig. 10). The spatial distribution of the VF values of the sub-basin ranged from 0.13 to 4.16. The VF values were classified into three classes: class 1 ($VF < 0.50$), class 2 ($0.50 \leq VF \leq 1.0$), and class 3 ($1.0 < VF \leq 4.46$) according to EI Hamdouni et al. (2008) (Fig. 11). The low VF values show that most valleys in the study area are V-shaped.

The values of the *I*_{at} were grouped into four classes according to the method of natural breaks to define the degree of the relative tectonic activity: class 1, very high tectonic activity with values of $S/n \leq 1.2$; class 2, high tectonic activity with values of $1.2 \leq S/n \leq 1.6$; class 3, moderate tectonic activity with values of $1.6 \leq S/n \leq 2$; and class 4, low tectonic activity with values of $2 \leq S/n$;

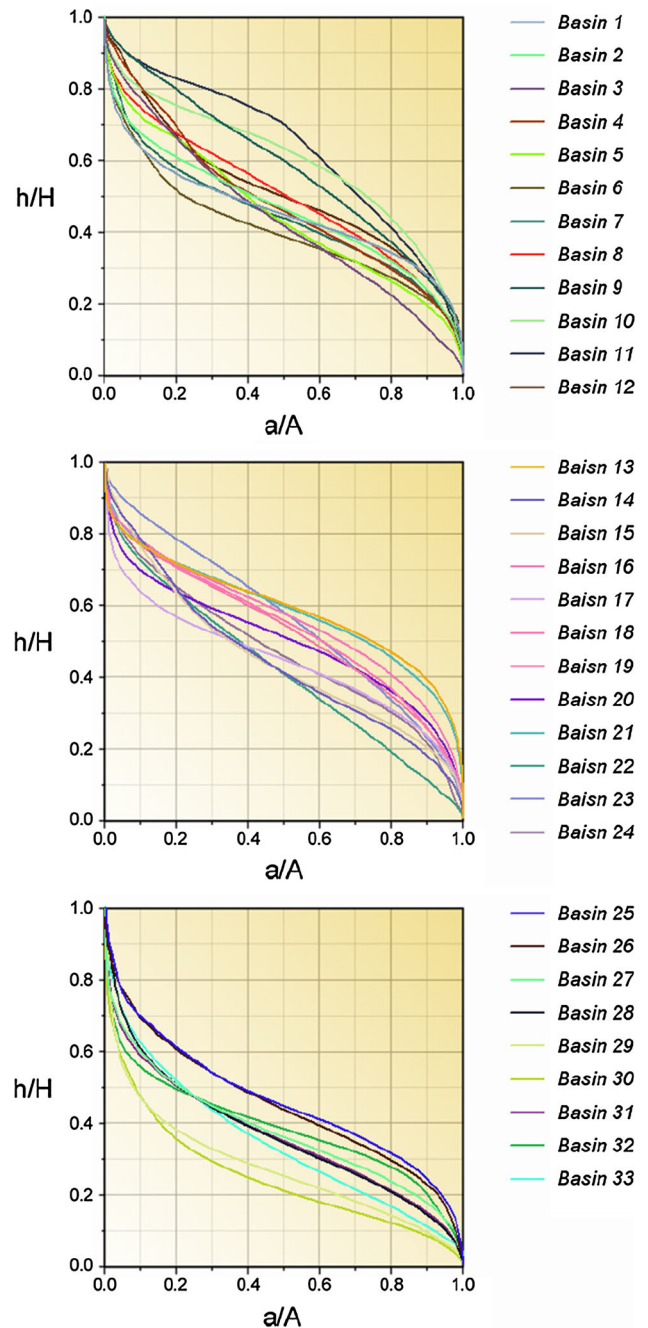


Fig. 8 Hypsometric curves of the study area

Table 2 shows the four classes of geomorphic indices and *I*_{at} classes of the study area. The distributions of the four *I*_{at} classes are shown in Fig. 12. Approximately 5.5 % of the study area (1463 km²) belongs to class 1; 54 % (14,343 km²) to class 2; 24.1 % (6417 km²) to class 3; and

Table 2 Classification of relative tectonic activity depending on geomorphic indexes

Basin no	SL	HI	AF	BS	VF	S/n	Iat
1	3	2	1	3	2	2.2	4
2	3	2	1	2	1	1.8	3
3	1	2	2	2	2	1.8	3
4	2	2	1	2	1	1.6	2
5	2	2	2	2	1	1.8	3
6	2	3	3	1	1	2.0	3
7	1	2	2	2	1	1.6	2
8	1	2	2	2	2	1.8	3
9	1	1	3	2	2	1.8	3
10	1	1	3	1	3	1.8	3
11	2	1	2	2	3	2.0	3
12	2	1	2	3	1	1.8	3
13	2	2	3	1	1	1.8	3
14	1	2	2	1	3	1.8	3
15	1	1	2	1	1	1.2	1
16	3	2	1	2	1	1.8	3
17	3	3	2	1	3	2.4	4
18	3	1	1	2	1	1.6	2
19	1	1	2	2	1	1.4	2
20	1	2	1	3	1	1.6	2
21	1	2	3	1	2	1.8	3
22	1	1	1	1	1	1.0	1
23	2	1	1	2	1	1.4	2
24	2	2	1	2	1	1.6	2
25	2	2	3	2	1	2.0	3
26	1	2	3	1	3	2.0	3
27	1	3	1	1	1	1.4	2
28	3	3	2	2	3	2.6	4
29	3	3	3	3	1	2.6	4
30	3	3	2	1	2	2.2	4
31	1	3	3	1	3	2.2	4
32	2	1	2	3	1	1.8	3
33	3	3	2	2	1	2.2	4

16.4 % (4363 km²) to class 4. The Iat tends to be low along the F3, F4, F5, and F6 fault zones.

Discussion of the difference among the tectonic activities

Previous studies of the evaluation of the relative active tectonics based on geomorphic indices mostly focused on a particular mountain front or small area (Bull and

McFadden 1977; Azor et al. 2002; Silva et al. 2003; EI Hamdouni et al. 2008). This investigation is an attempt to evaluate the relative active tectonics in a large area based on several sub-basins by using five geomorphic indices. The anomalous higher SL index in sub-basin 8, 19, and 23 were affected by the river and fault intersecting to form a high or perpendicular angle. The rock group is the same around the anomalous SL (Fig. 6). This can be interpreted to be tectonic signals that the rate of river incision was lower than the movement of the fault. There are lower SL indices when the river flows through the fault zone in parallel in sub-basin 28. This is the effect of an inactive strike-slip fault, as has been previously proposed in Central Taiwan (Lee and Tsai 2010). Figure 4b shows the distribution of the HI values in each of these rock groups. The mean HI values vary slightly, but the mean HI values are low in the basin floored with magmatic rocks with high resistance to erosion, mainly granites and diorites. In contrast, basins developed above siltstones, mudstones, and sandy conglomerates with lower erosion resistance have high mean HI values. Meanwhile, the error bars (standard deviations for each HI mean values) are high. Furthermore, this impact of the lithology is not enough to explain the variations in the relatively higher or lower HI values. The direction of tilting is mostly from west to east or southwest to northeast mostly (Fig. 9); it reflects the east-ward extrusion of Tibetan plateau.

The higher values of Iat with weak tectonic activity levels distribute mainly among the downstream of the study area (sub-basin 28, 29, 30, 31). The lower SL and HI values, concave hypsometric curves, and higher VF values in these basins reflect the weak role of tectonic uplift. The faults have little activity, and small earthquakes occur (Chen et al. 2007). In the south of the Bailongjiang, Minshan tectonic zone is a Quaternary fast uplift area deformed by the Minjiang fault (F11) and Huya fault (F12) (Fig. 2). It has a shielding effect to decrease the tectonic activity level of Longmenshan fault (F8, F9 and F10 in Fig. 2) (Deng et al. 1994). Due to this impact, the tectonic activity level of these faults decreased from the middle Pleistocene even to ceasing by the time of the late Pleistocene (Li et al. 2004, 2008; Chen et al. 2007, 2008).

The lower values of Iat with the strong tectonic activity levels distribute mainly among the upper reach of the studied basin. Several large earthquakes occurred here throughout history (Fig. 2), for example, the 8.0 magnitude earthquake of Wudu in 1879 (Zhan 2006). The study of the planation surface and river terraces reveals that the tectonic uplift amplitude is reduced from west to east. Although the sliding rate of some

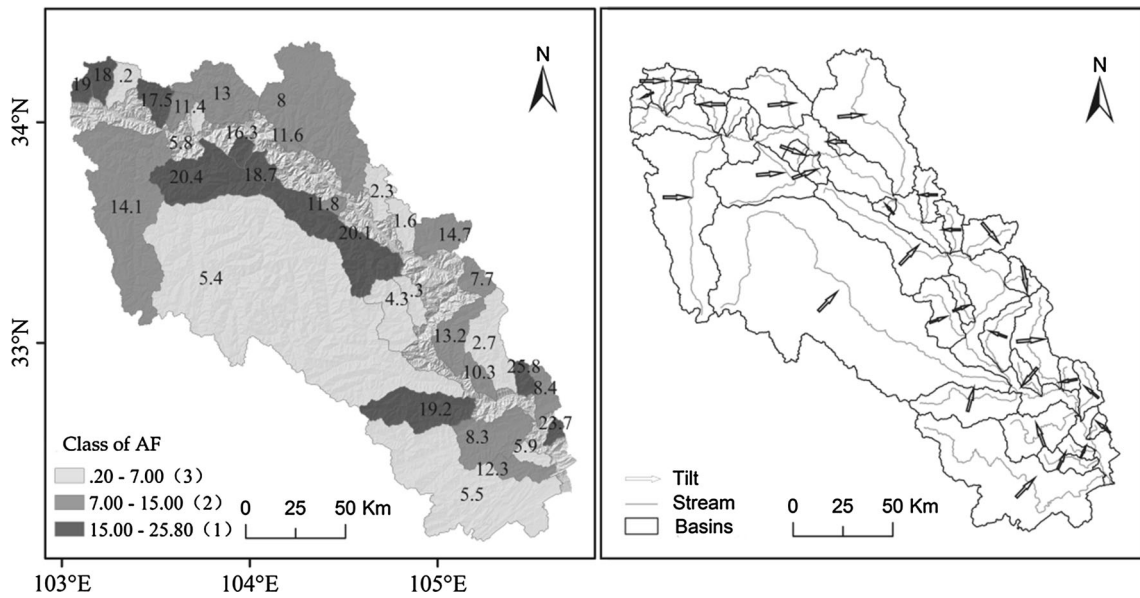


Fig. 9 The values of AF, classification, and inclination

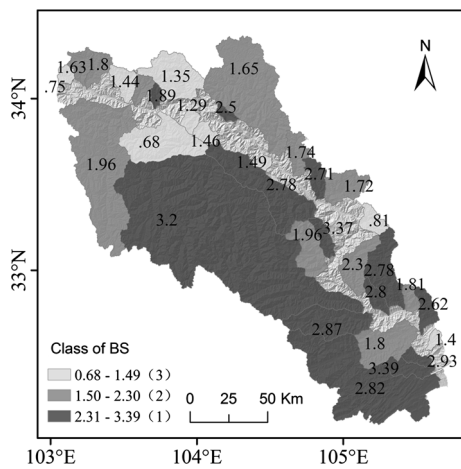


Fig. 10 The value of BS and classification

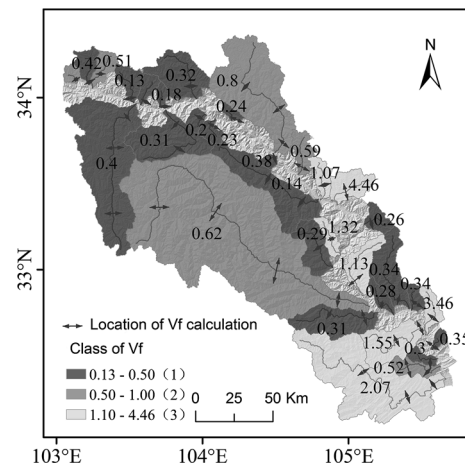


Fig. 11 The values of VF and classification

faults is still controversial (Yu et al. 2012), it is a fact that the region among F1–F2 is the transition of the deformation area where they play a part in the absorption and transformation of the movement between the East Kunlun fault and the West Qinling faults. Due to the tectonic uplift and the different velocity of the faults, the sub-basins here characterized have abnormal SL, high HI and AF values, convex hypsometric curves, and low VF values. Meanwhile, the tectonic activity degree will be enhanced in basins 19, 20, 21, and 22 for the extension to the

north of the Bailongjiang fault area by the rapid uplift process of Minshan (Zhang et al. 2010). To sum up, the result of the appraisal of the active tectonics in Bailongjiang basin is the same as the regional geological background.

The boundaries of most classes of geomorphic index follow the rule proposed by former researchers (EI Hamdouni et al. 2008). However, we only used five geomorphic indices instead of six, so the classes of IAT may be not

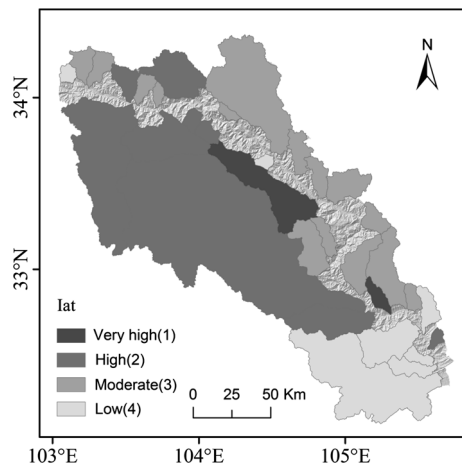


Fig. 12 Distribution of relative tectonic activity classes of Bailongjiang drainage basin

proper for the Bailongjiang basin. We used the method of natural breaks to classify the IAT to obtain the more appropriate result. The above discussion also proved that this method is right.

Conclusions

The geomorphic indices calculated from the GIS and remote sensing data are powerful tools to analyze the tectonic activity over a large area. We evaluated the relative tectonic activity using the DEM-derived drainage network and five geomorphic indices: stream-gradient index (SL), HI, drainage basin asymmetry (AF), drainage basin shape (BS), VF, and the modification of IAT.

The values of SL, HI, and BS were high along the major activity faults in the upstream and midstream of Bailongjiang, whereas the downstream have low values of SL, HI, and BS along inactive faults. The values of AF show widespread drainage basin asymmetry related to the eastward extrusion of the Tibetan Plateau. The values of VF show that many valleys are narrow and deep, suggesting a high rate of incision associated with tectonic uplift.

The low class 4 of Iat is primarily in the downstream of the Bailongjiang drainage basin, whereas the rest of the study area has moderate to very high active tectonics. In the study area, approximately 60 % of the total area, Iat is classified as 1 or 2, meaning high and very high tectonic activity levels. These areas distribute in the upstream and midstream of the Bailongjiang basin with the impact of uplift of the Tibetan Plateau and the activity faults. The downstream of the Bailongjiang basin has low activity

levels because of the low tectonic activity of the faults inhibited by Minshan. The results are consistent with the geological background.

Acknowledgments This research was fully supported by the National Natural Science Foundation of China (No. 40871010).

References

- Alipoor R, Pourkermani M, Zare M, El Hamdouni R (2011) Active tectonic assessment around Rudbar Lorestan dam site, High Zagros Belt (SW of Iran). *Geomorphology* 128(1):1–14
- Azor A, Keller EA, Yeats RS (2002) Geomorphic indicators of active fold growth: south Mountain-Oak Ridge Ventura basin, Southern California. *Geol Soc Am Bull* 114(6):745–753
- Bagha N, Arian M, Ghorashi M, Pourkermani M, El Hamdouni R, Solgi A (2014) Evaluation of relative tectonic activity in the Tehran basin, central Alborz, northern Iran. *Geomorphology* 213:66–87
- Bai SB, Wang J, Thiebes B, Cheng C, Chang ZY (2014) Susceptibility assessments of the Wenchuan earthquake-triggered landslides in Longnan using logistic regression. *Environ Earth Sci* 71(2):731–743
- Brookfield ME (1998) The evolution of the great river systems of southern Asia during the Cenozoic India–Asia collision: rivers draining southwards. *Geomorphology* 22(3–4):285–312
- Bull WB, McFadden LD (1977) Tectonic geomorphology north and south of the Garlock fault, California. In: Doehring DO (ed) *Geomorphology in Arid Regions*. Proceedings of the Eighth Annual Geomorphology Symposium. State University of New York, Binghamton, pp 115–138
- Chen HK, Li JJ (1997) General approach on geomorphologic evolution in Bailongjiang Basin since Quaternary. *J Chongqing Jiaotong Inst* 16(1):15–20
- Chen YC, Sung QC, Cheng KY (2003) Along-strike variations of morphometric features in the western foothills of Taiwan: tectonic implications based on stream gradient and hypsometric analysis. *Geomorphology* 56:109–137
- Chen GG, Ji FJ, Zhou RJ, Xu J, Zhou BG, Li XG, Ye YQ (2007) Primary research of activity segmentation of Longmenshan fault zone since late quaternary. *Seismol Geol* 29(3):657–673
- Chen LC, Chen J, Liu JF, Li F, Yang XP, Ran YK (2008) Investigation of late quaternary activity along the northern range-front fault, Longmenshan. *Seismol Geol* 30(3):710–722
- Cheng KY, Hung JH, Chang HC, Tsai H, Sung QC (2012) Scale independence of basin hypsometry and steady state topography. *Geomorphology* 171–172:1–11
- Dehbozorgi M, Pourkermani M, Arian M, Matkan AA, Motamedi H, Hosseiniasl A (2010) Quantitative analysis of relative tectonic activity in the Sarvestan area, central Zagros, Iran. *Geomorphology* 121:329–341
- Deng QD, Chen SF, Zhao XL (1994) Tectonics, Seismicity and dynamics of Longmenshan mountains and its adjacent regions. *Seismol Geol* 16(4):389–403
- El Hamdouni R, Irigaray C, Fernández T, Chacón J, Keller EA (2008) Assessment of relative active tectonics, southwest border of Sierra Nevada (Southern Spain). *Geomorphology* 96(1–2):150–173
- Font M, Amorese D, Lagarde JL (2010) DEM and GIS analysis of the stream gradient index to evaluate effects of tectonics: the Normandy intraplate area (NW France). *Geomorphology* 119(3–4):172–179

- Gao MX, Zeilinger G, Xu XW, Wang QL, Hao M (2013) DEM and GIS analysis of geomorphic indices for evaluating recent uplift of the northeastern margin of the Tibetan Plateau, China. *Geomorphology* 190(15):61–72
- Giaconia F, Booth-Rea G, Martínez-Martínez JM, Azañón JM, Pérez-Peña JV (2012a) Geomorphic analysis of the Sierra Cabrera, an active pop-up in the constructional domain of conjugate strike-slip faults: the Palomares and Polopos fault zones (eastern Betics, SE Spain). *Tectonophysics* 580:27–42
- Giaconia F, Booth-Rea G, Martínez-Martínez JM, Azañón JM, Pérez-Peña JV, Pérez-Romero J, Villegas I (2012b) Geomorphic evidence of active tectonics in the Sierra Alhamilla (eastern Betics, SE Spain). *Geomorphology* 146:90–106
- Grohmann CH, Riccomini C, Alves FM (2007) SRTM-based morphotectonic analysis of the Pocos de Caldas Alkaline Massif, southeastern Brazil. *Comput Geosci* 33(1):10–19
- Gu GX (1983) Catalogue of chinese earthquake. Science Press, Beijing, pp 778–824
- Guo JJ, Han WF, Liang SY, Li ZF (2006a) Study and comparison on the terrace of Taohe River and Minjiang River in Minxian–Dangchang area of the Western Qinling. *Geol Surv Res* 29(4):271–278
- Guo JJ, Han WF, Liang SY (2006b) Tectono-morphological evolution of the Minxian-Wudu area on the northeastern margin of the Qinghai–Tibet Plateau and plateau uplift. *Geol China* 33(2):383–392
- Hack JT (1973) Stream-profiles analysis and stream-gradient index. *J Res US Geol Surv* 1:421–429
- Hare PW, Gardner TW (1985) Geomorphic indicators of vertical neotectonism along converging plate margins, Nicoya Peninsula, Costa Rica; In: *Tectonic Geomorphology* (eds Morisawa M and Hack JT, Proceedings of the 15th Geomorphology Symposium, Birmingham, Allen and Unwin, Boston: 76–104
- Keller EA, Pinter N (1996) Active tectonics. Earthquakes, uplift and landscapes. Prentice Hall, Upper Saddle River, p 337
- Keller EA, Pinter N (2002) Active tectonics: earthquakes, uplift, and landscape, 2nd edn. Prentice Hall, Upper Saddle River
- Lee CS, Tsai LL (2010) A quantitative analysis for geomorphic indices of longitudinal river profile: a case study of the Choushui River, Central Taiwan. *Environ Earth Sci* 59(7):1549–1558
- Li CY (2005) Quantitative studies on major active fault zones in Northeastern Qinghai–Tibet Plateau. Ph. D. thesis (in Chinese). Beijing: Institute of Geology, China Earthquake Administration, 14–113
- Li JJ, Fang XM, Pan BT, Zhao ZJ, Song YG (2001) Late Cenozoic intensive uplift of Qinghai-Xizang Plateau and its impacts on environments in surrounding area. *Quat Sci* 21(5):2–12
- Li CY, Song FM, Ran YK (2004) Late quaternary activity and age constraint of the northern Longmenshan fault zone. *Seismol Geol* 26(2):248–257
- Li ZW, Liu SG, Chen HD, Liu S, Guo B, Tian XB (2008) Structural segmentation and zonation and differential deformation across and along the Longmen thrust belt, West Sichuan, China. *J Chengdu Univ Technol (Science & Technology Edition)* 35(4):440–454
- Liu BY (2012) Study on seismologic tectonic and mechanism on two M8 historical earthquakes at the southeastern area, Gansu province. Master thesis (in Chinese). Lanzhou: Lanzhou Institute of Seismology, China Earthquake Administration, 1–73
- Mahmood SA, Gloaguen R (2012) Appraisal of active tectonics in Hindu Kush: insights from DEM derived geomorphic indices and drainage analysis. *Geosci Front* 3(4):407–428
- Meng XM, Chen G, Guo P, Xiong MQ, Janusz W (2013) Research of landslides and debris flows in Bailong river basin: progress and prospect. *Mar Geol Quat Geol* 33(4):1–15
- Pedreira A, Pérez-Peña JV, Galindo-Zaldívar J, Azañón JM, Azor A (2009) Testing the sensitivity of geomorphic indices in areas of low-rate active folding (eastern Betic Cordillera, Spain). *Geomorphology* 105(3–4):218–231
- Pérez-Peña JV, Azañón JM, Azor A (2009a) CalHypso: an ArcGIS extension to calculate hypsometric curves and their statistical moments. Applications to drainage basin analysis in SE Spain. *Comput Geosci* 35(6):1214–1223
- Pérez-Peña JV, Azañón JM, Azor A, Delgado J, González-Lodeiro F (2009b) Spatial analysis of stream power using GIS: SLK anomaly maps. *Earth Surf Proc Land* 34(1):16–25
- Pérez-Peña JV, Azañón JM, Booth RG, Azor A, Delgado J (2009c) Differentiating geology and tectonics using a spatial autocorrelation technique for the hypsometric integral. *J Geophys Res* 114:F02018
- Pérez-Peña JV, Azor A, Azañón JM, Keller EA (2010) Active tectonics in the Sierra Nevada (Betic Cordillera, SE Spain): insights from geomorphic indexes and drainage pattern analysis. *Geomorphology* 119:74–87
- Ramírez-Herrera MT (1998) Geomorphic assessment of active tectonics in the Acambay graben, Mexican volcanic belt. *Earth Surf Proc Land* 23:317–332
- Ren JJ, Xu XX, Yeats RS, Zhang SM (2013) Millennial slip rates of the Tazang fault, the eastern termination of Kunlun fault: implications for strain partitioning in eastern Tibet. *Tectonophysics* 608:1180–1200
- Silva PG, Goy JL, Zazo C, Bardaji T (2003) Fault generated mountain fronts in Southeast Spain: geomorphologic assessment of tectonic and earthquake activity. *Geomorphology* 50(1–3):203–226
- Strahler AN (1952) Hypsometric (area–altitude) analysis of erosional topography. *Bull Geol Soc Am* 63:1117–1142
- Troiani F, Della Seta M (2008) The use of the stream length-gradient index in morphotectonic analysis of small catchments: a case study from Central Italy. *Geomorphology* 102(1):159–168
- Walcott RC, Summerfield MA (2008) Scale dependence of hypsometric integrals: an analysis of southeast African basins. *Geomorphology* 96(1–2):174–186
- Wells SG, Bullard TF, Menges CM, Drake PG, Karas PA, Kelson KI, Ritter JB, Wesling JR (1988) Regional variations in tectonic geomorphology along a segmented convergent plate boundary, Pacific coast of Costa Rica. *Geomorphology* 1(3):239–265
- Woerd JVD, Tapponier P, Ryerson FJ, Meriaux AS, Meyer B, Gaudemer Y, Finkel RC, Caffee MW, Zhao GG, Xu ZQ (2002) Uniform postglacial slip-rate along the central 600 km of the Kunlun Fault (Tibet), from ²⁶Al, ¹⁰Be, and ¹⁴C dating of riser offsets, and climatic origin of the regional morphology. *Geophys J Int* 48(3):356–388
- Yu JX, Zheng WJ, Yuan DY, Pang JZ, Liu XW (2012) Late quaternary active characteristics and slip-rate of Pingding-Huama fault, the eastern segment of Guanggaishan-dieshan fault zone (West Qinling Mountain). *Quat Sci* 32(5):957–967
- Yuan DY, Zhang PZ, Liu BC, Gan WJ, Mao FY (2004) Geometrical imagery and tectonic transformation of late quaternary active tectonics in Northeastern Margin of Qinghai–Xizang Plateau. *Acta Geol Sin* 78(2):270–278
- Zhan WW (2006) The research of engineering geological problems in the section of Gansu province of Lanzhou–Haikou highway. Lanzhou University Press, Lanzhou, pp 8–44
- Zhang YQ, Yang N, Chen W, Ma YS, Meng H (2003) Late Cenozoic tectonic deformation history of the east-west geomorphological boundary zone of china and uplift process of the eastern margin of the Tibetan Plateau. *Earth Sci Front* 10(4):599–612
- Zhang HP, Zhang PZ, Yuan DX, Zhen WJ, Zhen DW (2010) Differential landscape development of the central N-S seismic zone and its relation to the west Qinling tectonic belt. *Quat Sci* 30(4):803–811
- Zhang MS, Li ZH, Wang GL, Zhao C, Sun PP (2011) The geological hazard characteristics and exploration ideas of the Bailong River basin. *Northwest Geol* 44(3):1–9